Radiology Profile as a Potential Instrument to Differentiate Between Posterior Fossa Ependymoma (PF-EPN) Group A and B

Ushio Yonezawa[1], Vega Karlowee[3], Vishwa Jeet Amatya[2], Takeshi Takayasu[1], Motoki Takano[1], Yukio Takeshima[2], Kazuhiko Sugiyama[4], Kaoru Kurisu[1], Fumiyuki Yamasaki[1]

■ OBJECTIVE: **Posterior fossa ependymoma (PF-EPN) was categorized into PF-EPN-A and PF-EPN-B subgroups based on the DNA methylation profiling. PF-EPN-A was reported to have poorer prognosis compared with PF-EPN-B. In this study, we particularly evaluated preoperative imaging to distinguish PF-EPN-A from PF-EPN-B.**

■ METHODS: **Sixteen cases of PF-EPN were treated in our institution from 1999 to 2018. The patients were divided into PF-EPN-A and PF-EPN-B groups based on H3K27me3 immunostaining positivity. We evaluated progression-free survival, overall survival, as well as preoperative magnetic resonance imaging and computed tomography scan images in both groups. Based on T1WI and Gd-T1WI magnetic resonance images, the tumor contrast rate was determined from dividing the volume of gadolinium enhanced tumor by the overall tumor volume.**

■ RESULTS: **Nine cases (4 male, 5 female) were grouped as PF-EPN-A, and 7 (4 male, 3 female) as PF-EPN-B. The median age of PF-EPN-A and PF-EPN-B were 4 and 43 years old, respectively. In the PF-EPN-A group, the progression-free survival median value was 32.6 months, and the overall survival median was 96.9 months. In contrast, PFS in PF-EPN-B did not reach a median value ($P < 0.05$) and all the patients were alive ($P < 0.05$) at the end of the study. With imaging, tumor contrast rate in PF-EPN-B was more than 50% and significantly different from PF-EPN-A ($P = 0.0294$). Calcification was mainly observed in PF-EPN-A, whereas cystic formation was only seen in PF-EPN-B.**

■ CONCLUSIONS: **Contrast rate less than 50%, based on the magnetic resonance images, was characteristic in the PF-EPN-A group. Comparatively, cystic component and absence of calcification were more characteristic in the PF-EPN-B group.**

INTRODUCTION

Ependymoma is the third most common fourth ventricle tumor in pediatric patients, after pilocytic astrocytoma and medulloblastoma. Based on the recent development on the phenotype of methylation of CpG islands, regardless the World Health Organization (WHO) grading, posterior fossa (PF) ependymoma (EPN) was divided into group A (PF-EPN-A) and group B (PF-EPN-B).[1-3] PF-EPN-A is frequently found in infants and younger children, and PF-EPN-B is more common in older children, adolescents, and adults.[2,4-6]

The recent molecular subclassification added valuable information concerning patient prognosis. PF-EPN-A has poorer prognosis compared with PF-EPN-B despite patient age.[1,3,6-8] Furthermore, group B benefits more in less-aggressive therapy (referred to as de-escalation of therapy) compared with group A.[3,8,9] Therefore, we suggest that preoperatively distinguishing PF-EPN-A from PF-EPN-B has important clinical values in

Key words
- Contrast rate
- H3K27me3
- MR image
- Posterior fossa ependymoma

Abbreviations and Acronyms
ADC: Apparent diffusion coefficient
CT: Computed Tomography
DWI: Diffusion-weighted imaging
EPN: ependymoma
FLAIR: Fluid-attenuated inversion recovery
Gd: Gadolinium enhanced
MRI: Magnetic Resonance Imaging
OS: Overall survival
PF: Posterior fossa
PFS: Progression-free survival
T1WI: T1 weighted image
T2WI: T2 weighted image
WHO: World Health Organization

From the Departments of [1]Neurosurgery, and [2]Pathology, Graduate School of Biomedical and Health Sciences, Hiroshima University, Hiroshima, Japan; [3]Department of Pathological Anatomy, Diponegoro University, Semarang, Indonesia; and [4]Department of Clinical Oncology & Neuro-Oncology Program, Hiroshima University Hospital, Hiroshima, Japan

To whom correspondence should be addressed: Fumiyuki Yamasaki, M.D., Ph.D. [E-mail: fyama@hiroshima-u.ac.jp]

Citation: World Neurosurg. (2020) 140:e320-e327.
https://doi.org/10.1016/j.wneu.2020.05.063

Journal homepage: www.journals.elsevier.com/world-neurosurgery

Available online: www.sciencedirect.com

patient management planning. A study referring to this matter has not been established yet, however.

Additionally, in relation to prognosis, Bayliss et al reported on H3K27me3 reduction in poor prognosis for PF-EPN.[5] They suggested that low expression of H3K27me3 was due to aberrant DNA methylation. Panwalkar et al formulated that a global reduction of H3K27me3 expression in immunostaining was reliable in differentiating between PF-EPN-A and PF-EPN-B.[4]

In this study, we categorized our posterior fossa ependymoma cases into PF-EPN-A and B based on H3K27me3 immunostaining expression. Accordingly, we also evaluated preoperative imaging, clinical characteristics, and prognosis of each subgroup. Our study revealed that it is possible to distinguish PF-EPN-A from PF-EPN-B based on the tumor contrast rate ratio in non-enhanced T1-weighted imaging (T1WI) and gadolinium enhanced-T1WI (Gd-T1WI) magnetic resonance imaging (MRI) studies.

METHODS

This retrospective study was approved by the Hiroshima University Hospital review board (E-1601). Sixteen patients (8 male, 8 female), age range 1–69 years, with PF-EPN were treated in our institution from 1999 to 2018. Formalin-fixed paraffin embedded tissue were stained with routine hematoxylin and eosin for histopathologic diagnosis and grading. Both were reviewed by 2 pathologists based on the updated WHO 2016 classification.

Immunostaining was performed using automated immunostainers (BenchMark GX; Ventana Medical Systems, Tucson, AZ) as described in a previous publication.[10] An ultraView Universal DAB Detection Kit (760-500, Ventana Medical Systems) was used with cell conditioning (CC)-1 buffer (950-124, Ventana Medical Systems) for heat induced epitope retrieval treatment for 30 minutes. The primary antibodies were rabbit monoclonal anti-H3K27me3 (#9733, CST, Danvers, MA; 13.33 μg/mL) and mouse monoclonal anti-human Ki-67 antigen clone MIB-1 (F7268, Dako, Glostrup, Denmark; 40μg/mL). PF-EPN-A and PF-EPN-B grouping was based on the previous references, done by 3 blinded observers. Tumors with more than 20% negative cell was categorized as PF-EPN-A; and tumors with more than 80% positivity as B group.[4,5]

MRI study was performed using 2 different scanners: 1.5T or 3.0T. Patients from 1999 to June 2006 were examined with 1.5T (Signa Horizon Lx 1.5T, GE Medical Systems, Chicago, Illinois, USA). Patients from July 2007 to March 2017 were scanned with 3.0T (Signa Excite HD 3.0T, GE Medical Systems). Lastly, patients after March 2017 were examined with 3.0T (Philips Ingenia 3.0T CX, Philips Healthcare, Amsterdam, Netherlands). All patient underwent pre- and post-gadolinium enhanced (Gd) T1WI, T2-weighted (T2WI), fluid-attenuated inversion recovery (FLAIR), and diffusion-weighted imaging (DWI) with b value of 1000 s/mm^2. Regarding the apparent diffusion coefficient (ADC) map, the analysis of year 1999 to April 2017 period was done manually, whereas the period from March 2017 was included in the instrument analysis (Philips Ingenia 3.0T CX, Philips Healthcare). The manual ADC was done as followed: on b-1000 ADC maps, the regions of interest (ROIs) were manually placed on the central region of the enhanced tumor lesions, referring to the contrast-enhanced Gd-T1W1 images. The number of ROIs was depended on the size of the enhanced lesion. The ADC values of each tumor were then calculated based on 3–8 ROIs, and minimum absolute values were also obtained. The overall tumor volume and the gadolinium-enhanced tumor volume were determined using T1WI and Gd-T1WI images, respectively, utilizing a medical image viewer software (OsiriX, Pixmeo, Bernex, Switzerland). We made separate evaluations for the solid and the cystic components of the tumors. The contrast rate was determined by dividing the gadolinium enhanced component of the solid tumor volume by the overall solid tumor volume. Tumor calcification was examined using computed tomography (CT) scan image.

Statistical analyses were performed with SPSS version 19.0 (IBM SPSS Statistics, Version 19.0, Armonk, NY) and PRISM version 7.0 (GraphPad Software Inc, La Jolla, CA). The statistic features of patient age, sex, WHO grading, immunostaining results, preoperative CT and MRI findings including tumor location, calcification, ADC, progression-free survival (PFS) and overall survival (OS) were all examined. PFS and OS of both PF-EPN groups were compared using the non-parametric Kaplan-Meier survival analysis (log-rank test). The estimation of the PF-EPN A and B groups was based on the histologic and imaging characteristics. These data were evaluated by logistic regression analysis. The contrast rate of each group was compared by Mann-Whitney U test and Fisher's exact test. Statistical significance was assigned when $P < 0.05$.

RESULTS

Patient histopathologic profiles, imaging, and clinical characteristics are summarized in **Table 1**. Nine cases were categorized as PF-EPN-A and 7 cases as PF-EPN-B. Among PF-EPN-A, four patients were male, age ranging from 1 to 25 years (median age: 4 years; mean age: 6.7 years). There were 5 patients with EPN WHO grade II and 4 with anaplastic EPN WHO grade III. In the PF-EPN-B group, 4 patients were male, with an older range of ages, from 12–69 years, and higher median age (43 years) and mean age (44.9 years). This group has 6 patients with EPN WHO grade II and only 1 with anaplastic ependymoma WHO grade III.

The follow-up period median was 50 months for PF-EPN-A and 51 months for PF-EPN-B. Recurrence in PF-EPN-A was found in 5 cases (56%) with median PFS of 32.6 months. Four of 5 patients with tumor recurrence died with median OS of 96.9 months. On the contrary, the recurrence in PF-EPN-B was only found in 1 patient (14%) and all of the patients were alive during the follow-up period. The patient PFS and OS median values were significantly lower in the PF-EPN-A group compared with the PF-EPN-B group, with P value of 0.0360 and 0.0279, respectively (**Figure 1**).

We compared the differences between PF-EPN-A and PF-EPN-B based on the clinical, histopathologic, and imaging findings (**Table 2**). The age group in PF-EPN-A was significantly lower than PF-EPN-B ($P = 0.0402$, logistic regression analysis). With regard to histopathologic profile, although not statistically significant, the MIB-1 labeling index and patient number with WHO grade III (anaplastic EPN) were both higher in the PF-EPN-A group.

In terms of imaging characteristics, the contrast rate in the PF-EPN-B group was significantly different ($P = 0.0174$, Fisher's exact test) and higher ($P = 0.0404$) compared with the A group. We found that the contrast rate of all patients in the PF-EPN-B group

Table 1. Patient Histopathological Profile, Imaging, and Clinical Characteristics

				Histopathologic Profile			Imaging Characteristics							Clinical Characteristics			
Group	Age (years)	Sex	Resection	WHO Grade	H3K27me3	MIB-1 (%)	ADC	Enhanced Volume (cm^3)	Total Volume (cm^3)	Contrast Rate (%)	Ext. IVth	Cyst Volume (cm^3)	Calc.	PFS (months)	REC	OS (months)	Dead/ Alive
A	1	F	STR	III	+	15	0.949	30.3	34.12	88.8	+	0	+	4.6	1	21.7	dead
A	2	F	GTR	III	+	40	1.270	22.68	22.68	100	+	0	+	19.5	0	19.5	alive
A	2	M	PR	II	+	1	1.156	7.56	28.69	26.3	+	0	+	32	1	41.3	dead
A	3	F	GTR	II	+	70	0.748	5.58	29.8	18.7	–	0	+	19.4	1	62.8	alive
A	4	F	GTR	II	+	5	1.370	10.9	21.21	51.7	–	0	+	17.9	0	18.4	alive
A	4	F	GTR	II	+	15	1.123	7.54	20.17	37.4	–	0	–	32.6	1	53.3	dead
A	5	M	STR	III	+	20	NE	4.53	15.03	30.1	+	0	+	97.3	1	140.5	dead
A	14	M	GTR	II	+	1	1.452	0.27	9.57	2.8	+	0	–	204.5	0	204.5	alive
A	25	M	GTR	III	+	20	1.100	3.88	6.03	64.4	–	0	–	2.9	0	2.9	alive
B	12	M	STR	II	–	10	1.153	7.33	7.66	94.6	+	0	–	114	0	114	alive
B	30	M	GTR	II	–	5	1.331	11.46	11.46	100	–	0	–	193	0	193	alive
B	38	M	GTR	III	–	10	1.452	14.49	25.84	56.1	–	0	–	140.5	0	140.5	alive
B	43	M	GTR	II	–	3	1.263	14.5	16.71	86.7	+	0.51	–	23	1	122.5	alive
B	57	F	GTR	II	–	1	NE	5.11	8.75	58.4	–	1.82	+	78.2	0	78.2	alive
B	65	F	GTR	II	–	2	1.142	1.5	1.5	100	–	-	–	37.5	0	37.5	alive
B	69	F	GTR	II	–	3	1.021	9.41	9.91	94.8	–	-	–	78.2	0	78.2	alive

REC, recurrence; PFS, progression free survival; OS, overall survival; GTR, gross toral removal; STR, subtotal removal; PR, partial removal; Ext. IVth, extension outside IVth ventricle; ADC, apparent diffusion coefficient ($x10^{-3}cm^2/sec$); Calc, calcification; NE, not evaluable.

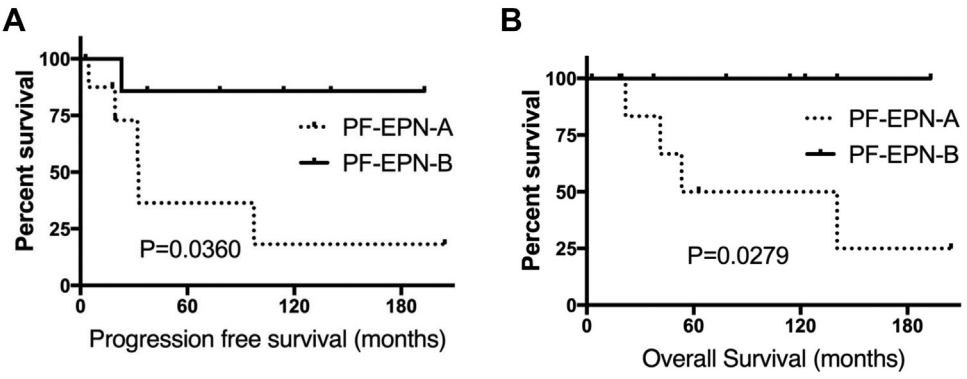

Figure 1. Kaplan-Meier curve of patient with posterior fossa ependymoma group A (PF-EPN-A) and B (PF-EPN-B). In the PF-EPN-A group, median progression-free survival (PFS) was 32.6 months and the median overall survival (OS) was 96.9 months. In the PF-EPN-B group, recurrence was observed in only 1 patient and PFS did not reach a median value. The PFS was statistically shorter in PF-EPN-A group ($P = 0.0360$, log-rank test), and the OS was also statistically shorter in PF-EPN-A ($P = 0.0279$, log-rank test).

was more than 50%; whereas in the PF-EPN-A group, only 5 of 9 patients had a contrast rate greater than 50%. The typical imaging features of PF-EPN-A was low contrast rate with calcification on CT scan, whereas the typical PF-EPN-B showed high contrast rate, without calcification, and sometimes with cystic lesions. In relation to the WHO grading, the median value of contrast rate in the PF-EPN-A group with WHO grade III was higher (30.1% to 100%, median 76.6%) than grade II (2.8% to 51.7%, median 26.3%). The statistical difference was not significant (P = 0.0635, Mann Whitney U test), however, considering the small sample size.

Other imaging characteristics were also evaluated in this study. ADC values were not significantly different between the 2 groups. Cystic formation was observed only in PF-EPN-B, and calcification was observed only in PF-EPN-A. Statistical differences were not observed in either imaging characteristic, however. Tumor volume and extension to the outside area of the fourth ventricle were also not statistically significant between both groups. Representative cases of PF-EPN-A (**Figure 2**) and PF-EPN-B (**Figure 3**) are presented.

Then, we compared the difference between PF-EPN-A and PF-EPN-B in clinical, imaging, and histologic findings (**Table 2**). The age of patients in the PF-EPN-A group was statistically lower than in the PF-EPN-B group (P = 0.0402, logistic regression analysis). MIB-1 labeling index was higher in PF-EPN-A and diagnosis of WHO grade III (anaplastic EPN) was more common in PF-EPN-A, yet these parameters did not reach statistical significance.

In PF-EPN-B, the contrast rate was higher than 50% in all patients, whereas in the PF-EPN-A group, it was lower than 50% in 5 of 9 patients. A significant statistical difference was observed between PF-EPN-A and PF-EPN-B contrast rate (P = 0.0174, Fisher's exact test). Logistic regression analysis also showed that the contrast rate was higher in PF-EPN-B compared with PF-EPN-A (P = 0.0404). The typical imaging feature of PF-EPN-A was a low contrast rate and calcification on simple CT, while the typical PF-EPN-B showed a high contrast rate, without calcification, and sometimes with cystic lesions. Among the PF-EPN-A group, we divided the patients into WHO grade II and grade III groups. The contrast rate of grade II PF-EPN-A was 2.8% to 51.7% (median: 26.3%), whereas that of grade III PF-EPN-A was 30.1% to 100% (median: 76.6%). The statistical difference was did not reach significance (P = 0.0635, Mann-Whitney U test) because of the small sample size.

Other imaging characteristics were also evaluated in this study. ADC values were not significantly different between the 2 groups. Cystic formation was observed only in PF-EPN-B, and calcification was observed only in PF-EPN-A. However, statistical differences were not observed in these imaging characteristics. Other factors, including tumor volume or extension to the outside area of the IVth ventricle, were not statistically significant either between PF-EPN-a and PF-EPN-B. Representative cases of PF-EPN-A (**Figure 2**) and PF-EPN-B (**Figure 3**) were presented.

We also contrasted both groups based on the histopathological profile, imaging and clinical characteristics (**Table 2**). As we mentioned before, the age group in PF-EPN-A was significantly lower than PF-EPN-B (P = 0.0402, logistic regression analysis). In regard to histopathological profile, although not statistically significant, the MIB-1 labeling index and patient number with WHO grade III were both higher in PF-EPN-A. In imaging characteristic analysis, the contrast rate in PF-EPN-B subgroup was significantly different (P = 0.0174, Fisher exact test) and higher (P = 0.0404). We found that the contrast rate of all patients in PF-EPN-B group was higher than 50%. Whereas in PF-EPN-A group, only 5 of 9 patients with contrast rate higher than 50%. Concerning with WHO grading in PF-EPN-A subgroup, the median value of the contrast rate in tumor with WHO grade III was higher (30.1 to 100%, median of 76.6%) than grade II (2.8 to 51.7%, median value of 26.3).

Table 2. Comparison of PF-EPN-A and PF-EPN-B Subgroups

	Posterior Fossa Ependymoma-A	Posterior Fossa Ependymoma-B	Logistic Analysis
Patient Number	9	7	
Age, years			
range	1—25	12—69	
mean/median	6.7/4	44.9/43	0.0402*
Sex			
male/female	4/5	4/3	0.6153
Histopathologic profile			
MIB-1 labeling index, %			
mean (range)	21 (1—70)	5 (1—10)	0.1047
WHO grade II	5	6	
WHO grade III	4	1	0.2173
Imaging characteristic			
Contrast rate			
50% or higher	4	7	0.0294†
mean	46.69%	79.79%	0.0404*
Calcification			
case number	6	1	0.0543
Extension beyond fourth ventricle			
case number	5	2	0.288
Apparent diffusion coefficient ($x10^{-3}$ mm^2/sec)			
range	0.748—1.452	1.000—1.452	
mean/median	1.146/1.139.5	1.205/1.207.5	0.4381
Cystic component			
case number	0	2	0.9789
Tumor volume (cm^2)	20.81	14.67	0.0775

*Significant difference ($P < 0.05$).
†Fisher's exact test.

DISCUSSION

In pediatric brain tumors, there have been many advances in identifying imaging characteristics to distinguish EPN from embryonal tumors.[11-15] However, compared with medulloblastoma, in which the imaging phenotypes (i.e., tumor location, enhancement pattern, and dissemination) were related to the molecular subgroups, there have thus far been no similar studies focusing on EPN.[16-18] Based on our results, the imaging characteristics of PF-EPN-A and PF-EPN-B are distinguishable. PF-EPN-B was markedly enhanced by gadolinium with high contrast rate. Conversely, the enhancement was lower in PF-EPN-A. Some PF-EPN-A patients may also have calcification.

Pertaining to patient management, PF-EPN-B is known to have favorable 10-year overall survival, with a subset of patients being able to be cured by only gross total removal.[3,6] Moreover, the recurrence rate of PF-EPN-B was low even in patients with incomplete resection.[1-6,19] On the contrary, in a a subset of patients, PF-EPN-A would recur after adjuvant irradiation and might have less advantage of gross total removal.[6,8] In these circumstances, our finding provides valuable clinical information for patient management in neurosurgery. Primarily, this would be beneficial for the tumor removal procedure in cases with vital structure adhesion (e.g., brainstem and cranial nerves). For instance, a neurosurgeon may not need to make any unnecessary attempt to remove a tumor completely, with regard to the risk of causing disabilities to the patient, in cases that are already known to be PF-EPN-B.

A study by Pajtler et al utilizing DNA methylation profiling identified 9 molecular subgroups in EPN based on risk stratification, over the conservative WHO grading.[2] Overall, they divided EPN into 3 groups based on the location: supratentorial, posterior fossa, and spine. Each group was further divided into 3 subgroups. Concerning the PF-EPN group, the subgroups were

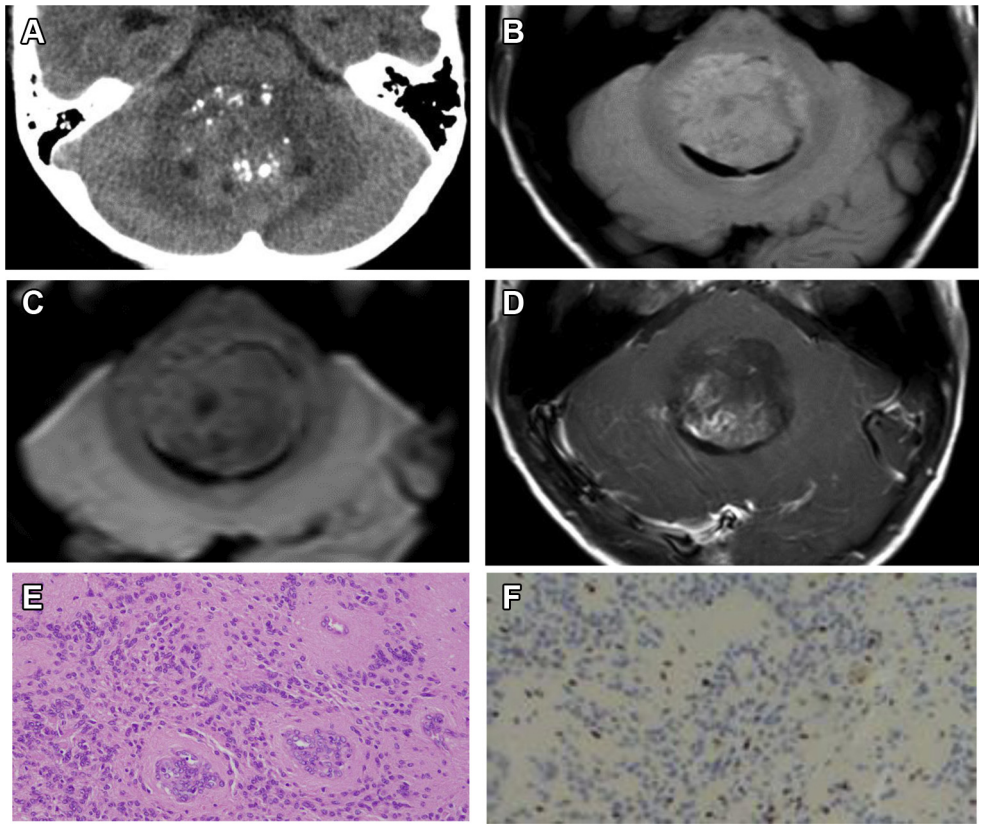

Figure 2. A 4-year-old girl with posterior fossa ependymoma-A (PF-EPN-A). Based on the imaging, the tumor was located in the fourth ventricle. (**A**) Axial plain CT showed calcification deposit in the tumor. (**B**) Axial FLAIR MRI revealed a high-intense tumor. (**C**) The tumor appeared iso-to low-intense on DWI image. (**D**) Gd-T1WI image showed partial enhancement, with tumor contrast rate of 37.4%. (**E**) Routine histopathological analysis revealed diffuse proliferation of ependymal tumor cells with perivascular pseudorosette structures, consistent with ependymoma WHO grade II. (**F**) H3K27me3 immunostaining was concluded as negative.

subependymoma balanced genome (PF-EPN-SE), ependymoma balanced genome (PF-EPN-A), and ependymoma chromosomal instability (PF-EPN-B).

In term of PF-EPN, previous studies by Witt et al and Mack et al addressed fundamental characteristic distinctions between PF-EPN-A and PF-EPN-B.[1,3] Both studies observed that PF-EPN-A patients are younger with poorer prognosis (e.g., recurrence, metastasis, survival rate) compared with PF-EPN-B patients.[3] Based on gene set enrichment analysis, Witt et al recognized that there were many cancer-related mechanisms in group A (e.g., PDGF signaling, MAPK signaling, EGFR signaling) whereas group B was delineated by gene in ciliogenesis/microtubule assembly and mitochondria/oxidative metabolism.[3] Correspondingly, Mack et al disclosed that the hyperactivity of PRC2 complex may lead to tumor suppressor gene silencing by DNA CpG hypermethylation in PF-EPN-A. This same study also suggested that an ongoing hypermethylation of promoter CpG islands and H3K27 may contribute to this subgroup tumor maintenance.[1]

In accordance with the Mack et al study, Panwalkar et al utilized immunostaining in an attempt to find a simplified tool to detect the H3K27me3 mutation in PF-EPN-A and PF-EPN-B subgroups.[1,4] That study sufficiently found that H3K27me3 immunostaining has 99% sensitivity and 100% specificity to categorize between the 2 subgroups.[4] Our H3K27me3 immunostaining data also showed the same characteristics in age and WHO grading in both subgroups. In our study, imaging information including tumor location at posterior fossa (e.g., extension of foramen of Luschka and/or Magendie), tumor size, cystic formation, and even ADC calculation could not differentiate PF-EPN-A and PF-EPN-B. PF-EPN-B ependymoma showed characteristics of high contrast rate, however, which is useful for differentiation of PF-EPN-B from PF-EPN-A. No calcification at CT may also help for the differentiation of molecular subtype of ependymoma, which is specific characteristics of PF-EPN-A (sensitivity 66.7%, specificity 85.7%). Increase contrast rate from grade 2 to grade 3 in PF-EPN-A may be associated with breaking the blood–brain barrier, which is consistent with the imaging characteristics of diffuse glioma.[20]

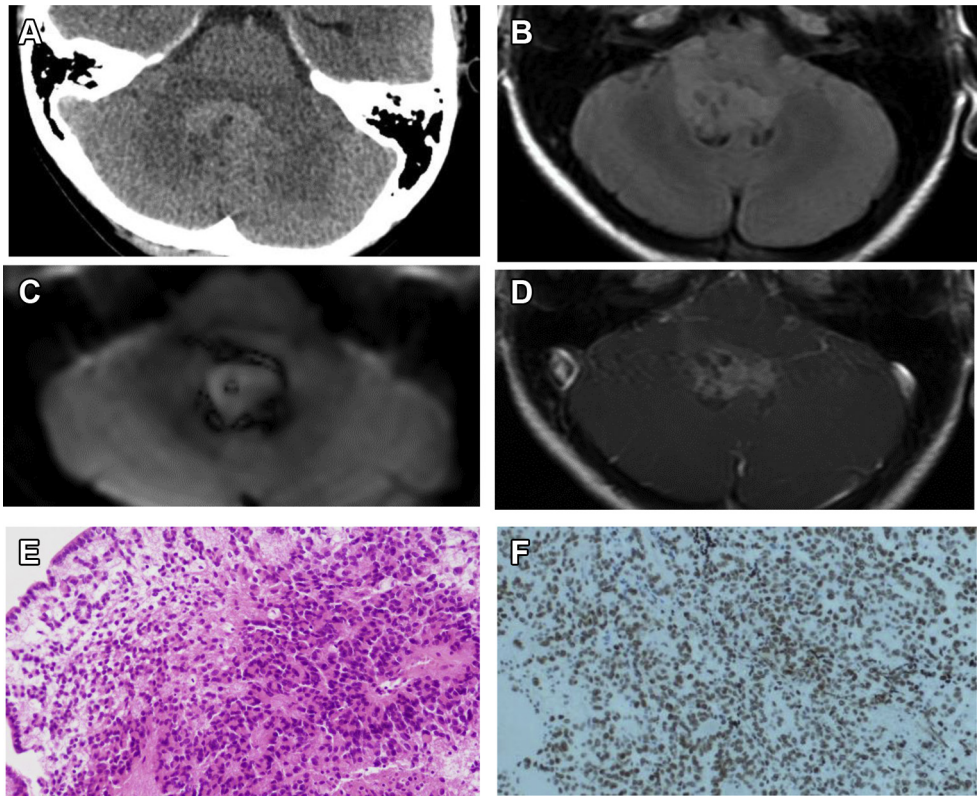

Figure 3. A 12-year-old boy with posterior fossa ependymoma-B (PF-EPN-B). (**A**) The tumor was located in the fourth ventricle, with no calcification on CT image. (**B**) MRI FLAIR axial exhibited a high-intensity tumor, with small cysts, extended laterally through the right foramen of Luschka. (**C**) On DWI axial, the tumor appeared of relatively high intensity. (**D**) Gd-T1WI showed homogenous enhancement with contrast rate of 95.6%. (**E**) Routine hematoxylin and eosin staining indicated ependymal tumor with moderate cellularity and perivascular pseudorosettes structures, consistent with ependymoma WHO grade II. (**F**) H3K27me3 immunostaining was retained.

Increased contrast rate may prevent the accuracy of differential diagnosis of PF-EPN-A from PF-EPN-B, however.

In short, our methods of calculating contrast rate of tumor would be useful for the diagnosis of WHO grade II PF-EPN-A. Another study on medulloblastoma using gadolinium enhancement showed the usefulness of differential diagnosis of group 4 medulloblastoma from other subgroups, as medulloblastoma group 4 is characterized by a minimal/no enhancement pattern.[17] This result about medulloblastoma also supports the fact that epigenetic features could appear in the degree of tumor enhancement, which is consistent with the imaging characteristics of PF-EPN.

With regard to imaging characteristics, Zhao et al observed that MRI gadolinium enhancement was valuable to categorize medulloblastoma into their 4 molecular groups. The characteristics were based on the tumor location, enhancement pattern, and dissemination.[17] Those results refined the fact that the degree of tumor enhancement was also influenced by the tumor epigenetic characteristic. In this study, we utilized T1WI and Gd-T1WI MRI and found that the PF-EPN-B group retained a higher contrast rate than the PF-EPN-A group. We acknowledge that contrast rate increase may also be detected in PF-EPN-A with advancement from WHO grade II to grade III. This event is related to blood–brain barrier disruption, and also similarly found in diffuse glioma.[20] This circumstances may impede the accuracy of using the method. Therefore, this method would be more effective in EPN WHO grade II. Additionally, CT scan findings of calcification also contributed in distinguishing between the PF-EPN-A and PF-EPN-B subgroups. Differently from PF-EPN-B, PF-EPN-A retained calcification formation in the tumor (sensitivity 66.7%, specificity 85.7%). However, we did not find that other imaging characteristics, such as tumor extension to the foramen of Luschka and/or Magendie, tumor size, cystic formation, even ADC rate, were different between PF-EPN-A and PF-EPN-B subgroups.

There were some limitations regarding our study. The study population was limited, so it is difficult to form a definitive conclusion. Subsequently, future studies are necessary to confirm the utility of our findings. Additionally, concerning PF-EPN-A and PF-EPN-B subgroup differentiation, we also aware that H3K27me3

immunostaining is subpar compared with DNA methylation analysis. Nevertheless, this method is more suitable for routine diagnosis. Overall, our study shows that it is possible to make a distinction preoperatively between PF-EPN-A and PF-EPN-B, particularly in EPN WHO grade II. We argue that because of the different prognoses between the 2 subgroups, this finding provide valuable clinical information in patient management, specifically in tumor resection precautionary measures.

CONCLUSIONS

In this study, we showed that a contrast rate less than 50%, based on T1WI and Gd-T1WI MRI, as a characteristic in PF-EPN can help to indicate PF-EPN-A subgrouping. Comparatively, a cystic component and absence of calcification can indicate PF-EPN-B subgrouping. We believe that this simple method may contribute to the preoperative working diagnosis as well as patient management planning.

CRediT AUTHORSHIP CONTRIBUTION STATEMENT

Ushio Yonezawa: Conceptualization, Methodology, Formal analysis, Writing - original draft. **Vega Karlowee:** Investigation, Writing - review & editing. **Vishwa Jeet Amatya:** Data curation, Investigation. **Takeshi Takayasu:** Data curation, Investigation. **Motoki Takano:** Data curation, Investigation. **Yukio Takeshima:** Data curation, Investigation. **Kazuhiko Sugiyama:** Supervision, Writing - review & editing. **Kaoru Kurisu:** Supervision, Writing - review & editing. **Fumiyuki Yamasaki:** Conceptualization, Validation, Writing - review & editing.

REFERENCES

1. Mack SC, Witt H, Piro RM, et al. Epigenomic alterations define lethal CIMP-positive ependymomas of infancy. *Nature*. 2014;506:445-450.
2. Pajtler KW, Witt H, Sill M, et al. Molecular classification of ependymal tumors across all cns compartments, histopathological grades, and age groups. *Cancer Cell*. 2015;27:728-743.
3. Witt H, Mack SC, Ryzhova M, et al. Delineation of two clinically and molecularly distinct subgroups of posterior fossa ependymoma. *Cancer Cell*. 2011;20:143-157.
4. Panwalkar P, Clark J, Ramaswamy V, et al. Immunohistochemical analysis of H3K27me3 demonstrates global reduction in group-A childhood posterior fossa ependymoma and is a powerful predictor of outcome. *Acta Neuropathol*. 2017;134:705-714.
5. Bayliss J, Mukherjee P, Lu C, et al. Lowered H3K27me3 and DNA hypomethylation define poorly prognostic pediatric posterior fossa ependymomas. *Sci Transl Med*. 2016;8:366ra161.
6. Ramaswamy V, Hielscher T, Mack SC, et al. Therapeutic impact of cytoreductive surgery and irradiation of posterior fossa ependymoma in the molecular era: a retrospective multicohort analysis. *J Clin Oncol*. 2016;34:2468-2477.
7. Pajtler KW, Mack SC, Ramaswamy V, et al. The current consensus on the clinical management of intracranial ependymoma and its distinct molecular variants. *Acta Neuropathol*. 2017;133:5-12.
8. Khatua S, Mangum R, Bertrand KC, Zaky W, McCall D, Mack SC. Pediatric ependymoma: current treatment and newer therapeutic insights. *Future Oncol*. 2018;14:3175-3186.
9. Cage TA, Clark AJ, Aranda D, et al. A systematic review of treatment outcomes in pediatric patients with intracranial ependymomas. *J Neurosurg Pediatr*. 2013;11:673-681.
10. Karlowee V, Amatya VJ, Takayasu T, et al. Immunostaining of increased expression of enhancer of zeste homolog 2 (EZH2) in diffuse midline glioma H3K27M-mutant patients with poor survival. *Pathobiology*. 2019;86:152-161.
11. Yamasaki F, Kurisu K, Satoh K, et al. Apparent diffusion coefficient of human brain tumors at MR imaging. *Radiology*. 2005;235:985-991.
12. Rumboldt Z, Camacho DL, Lake D, Welsh CT, Castillo M. Apparent diffusion coefficients for differentiation of cerebellar tumors in children. *AJNR Am J Neuroradiol*. 2006;27:1362-1369.
13. Gimi B, Cederberg K, Derinkuyu B, et al. Utility of apparent diffusion coefficient ratios in distinguishing common pediatric cerebellar tumors. *Acad Radiol*. 2012;19:794-800.
14. Koral K, Mathis D, Gimi B, et al. Common pediatric cerebellar tumors: correlation between cell densities and apparent diffusion coefficient metrics. *Radiology*. 2013;268:532-537.
15. Takayasu T, Yamasaki F, Akiyama Y, et al. Advantages of high b-value diffusion-weighted imaging for preoperative differential diagnosis between embryonal and ependymal tumors at 3T MRI. *Eur J Radiol*. 2018;101:136-143.
16. Perreault S, Ramaswamy V, Achrol AS, et al. MRI surrogates for molecular subgroups of medulloblastoma. *AJNR Am J Neuroradiol*. 2014;35:1263-1269.
17. Zhao F, Li C, Zhou Q, et al. Distinctive localization and MRI features correlate of molecular subgroups in adult medulloblastoma. *J Neurooncol*. 2017;135:353-360.
18. AlRayahi J, Zapotocky M, Ramaswamy V, et al. Pediatric brain tumor genetics: what radiologists need to know. *Radiographics*. 2018;38:2102-2122.
19. Zapotocky M, Beera K, Adamski J, et al. Survival and functional outcomes of molecularly defined childhood posterior fossa ependymoma: cure at a cost. *Cancer*. 2019;125:1867-1876.
20. Verburg N, Hoefnagels FWA, Barkhof F, et al. Diagnostic accuracy of neuroimaging to delineate diffuse gliomas within the brain: a meta-analysis. *AJNR Am J Neuroradiol*. 2017;38:1884-1891.

Conflict of interest statement: The authors declare that the article content was composed in the absence of any commercial or financial relationships that could be construed as a potential conflict of interest.

Received 24 February 2020; accepted 8 May 2020

Citation: World Neurosurg. (2020) 140:e320-e327.
https://doi.org/10.1016/j.wneu.2020.05.063

Journal homepage: ***www.journals.elsevier.com/world-neurosurgery***

Available online: ***www.sciencedirect.com***